NASA

MEMORANDUM

INVESTIGATION ON THE USE OF A FREELY ROTATING ROTOR AT

THE COWL FACE OF A SUPERSONIC CONICAL INLET TO

REDUCE INLET FLOW DISTORTION

By Theodore J. Goldberg and Emanuel Boxer

Langley Research Center
Langley Field, Va.

NATIONAL AERONAUTICS AND
SPACE ADMINISTRATION

June 1959
Declassified July 11, 1961

NATIONAL AERONAUTICS AND SPACE ADMINISTRATION

MEMORANDUM 5-28-59L

INVESTIGATION ON THE USE OF A FREELY ROTATING ROTOR AT

THE COWL FACE OF A SUPERSONIC CONICAL INLET TO

REDUCE INLET FLOW DISTORTION

By Theodore J. Goldberg and Emanuel Boxer

SUMMARY

An investigation has been made on the use of a freely rotating rotor at the cowl face of a supersonic conical diffuser to determine its effectiveness in reducing inlet flow distortion and the penalty in terms of total-pressure loss imposed by such a device when distortions are negligible. Tests were made with a rotor having an inlet tip diameter of 2.18 inches and a ratio of hub radius to tip radius of 0.52, in conjunction with a conical inlet having a 25° semivertex cone angle, at a Mach number of 2.1 over an angle-of-attack range of 0° to 8°.

A simplified analysis showing that a supersonic, freely rotating rotor with maximum solidity for noninterference between blades will operate in an undistorted flow with a total-pressure defect of 1 percent or less was experimentally verified. Overall total-pressure distortions of 0.1 to 0.4 and Mach number distortions of 0.4 to 1.4, obtained at 4° to 8° angle of attack, were reduced about 30 percent and 23 percent, respectively, because of the presence of the rotor, with no measurable total-pressure loss. The rotor increased the peak total-pressure recovery at the simulated combustion chamber $1\frac{1}{2}$ and $3\frac{1}{2}$ percent at 6° and 8° angles of attack, respectively. This increase is attributed to lower diffusion duct losses as a consequence of a more uniform flow created by the rotor.

INTRODUCTION

In performing its role as a component of the overall powerplant installation, one of the requirements of the air-intake system is to

deliver the flow with uniform total pressure or velocity at the compressor inlet. The presence of airflow distortion at the discharge of the air-intake system has impaired to some extent the performance of many current subsonic and transonic airplanes.

The causes of flow distortion, a condition which is characterized by total-pressure variations and, consequently, nonuniform velocity profiles either radially, circumferentially, or a combination of the two, are somewhat dependent upon flight speed. At subsonic flight speeds, air generally enters the inlet with little distortion. Such distortions as manifest themselves at the diffuser discharge therefore arise from local boundary-layer growth and separation near the duct walls. At supersonic flight speeds, the problem is further complicated by the existence of added distortions near the inlet throat. These distortions are caused primarily by nonuniform supersonic compression which may occur because of interaction between the inlet terminal shock and the compression-surface boundary layer, by operation at subcritical mass flow with subsequent entrance of a vortex sheet into the inlet, or by operation at angle of attack or yaw.

The detrimental effects of inlet flow distortions on thrust, altitude operating limits, and acceleration potential of jet engines have been well documented in references 1 to 5. Because of the importance of this problem, much effort is being devoted to correct or minimize the effects of distortion. At present, attempts are being made to design compressors to accept and operate with a distorted inlet flow (refs. 6 and 7). This essentially is a long-range program primarily because of the lead time necessary to produce a jet engine. Methods to reduce distortion by such means as long mixing ducts, divergent-convergent portions of the diffuser, vortex generators, installation of screens, and the use of freely rotating wheels have been investigated and reported in references 8 to 13. These devices operate on the flow at low Mach number after nearly complete diffusion where the distortion is well formed.

The present paper proposes the use of a freely rotating rotor at the cowl face of an axisymmetric supersonic spike diffuser to reduce the flow distortion originating ahead of the subsonic diffuser. The manner in which a freely rotating blade row acts to reduce velocity distortion has been described in reference 11 in which it was noted that in regions of high velocity (generally higher stagnation pressure) the blades act as a turbine extracting energy and transfer this energy by compressor action to regions of low velocity with no net work except for that required to overcome bearing friction. Because of the geometry concerned, the use of the rotor is restricted to conical-type inlets.

An investigation was made to determine the capability of a freely rotating blade row at the cowl face of a supersonic conical diffuser to reduce inlet distortion and to determine the penalty imposed by such a

device when distortions are not present. An analysis using simplified criteria based largely upon one-dimensional momentum calculations and two-dimensional linearized airfoil theory was made to determine the total-pressure loss in undistorted flow. Tests were made in which a 2.18-inch-diameter freely rotating rotor was used in conjunction with a single-cone diffuser at a Mach number of 2.1 for an angle-of-attack range of 0° to 8°. Total pressures were measured 7 inches behind the cowl lip and at the simulated combustion chamber to determine the distortion and pressure recovery with and without the rotor.

SYMBOLS

A	flow area, ft^2
a	velocity of sound, fps
C_D	total drag coefficient
$C_{D,o}$	profile drag coefficient
C_F	axial-force coefficient, $\dfrac{F_a}{\gamma p_1 A}$
C_f	friction coefficient
C_L	lift coefficient
c	chord, ft
D	drag per blade, lb
F	force, lb
G	blade spacing, $2\pi r/n$, ft
L	lift per blade, lb
M	Mach number
$\dfrac{\Delta M}{M}$	Mach number distortion defined as ratio of difference between maximum and minimum values of Mach number to arithmetical average value of Mach number as measured by rakes at station 3

n   number of blades

p   pressure, lb/ft^2

$\dfrac{\Delta p_t}{p_t}$ total-pressure distortion defined as ratio of difference between maximum and minimum values of total pressure to arithmetical average value of total pressure as measured by rakes at station 3, $\dfrac{\left(p_{t,3}\right)_{max} - \left(p_{t,3}\right)_{min}}{\left(p_{t,3}\right)_{av}}$

R   gas constant, $ft^2/sec^2 \text{-}^oR$

r   radius, ft

r_b center-body radius, in.

r_c cowling radius, in.

T   temperature, ^oR

t   thickness, ft

V   velocity, fps

X   axial distance from cowl lip, in.

x   axial distance from center-body tip, in.

α angle of attack, deg

β air inlet angle, deg

γ ratio of specific heats

ϵ shock-wave angle measured from upstream flow direction, deg

θ angular coordinate of meridional plane, deg (measured from top in a clockwise direction looking downstream)

ρ gas density, slugs/cu ft

σ solidity, ratio of blade chord to blade spacing

σ_m maximum solidity for noninterference between blades

ϕ blade setting angle, deg

Subscripts:

a   axial component parallel to axis of rotation

av   arithmetical average

cr   critical

max   maximum

min   minimum

t   stagnation conditions

u   tangential component

0   settling chamber

1   rotor inlet

2   rotor exit

3   measuring station downstream of rotor

4   measuring station at simulated combustion chamber

ANALYSIS OF FREELY ROTATING ROTOR IN UNDISTORTED FLOW

The usefulness of any device to reduce distortion is dependent upon the penalty imposed in terms of total-pressure loss across such a device when distortions are negligible or nonexistent as well as its ability to reduce distortion. No matter how successful the device may be for reducing distortion, its use cannot be tolerated if the pressure drop is excessive since a 1-percent total-pressure loss results in a reduction in thrust of as much as $1\frac{1}{2}$ percent for a turbojet engine (ref. 14). The supersonic freely rotating wheel is one device whose pressure loss in an undistorted stream is amenable to analytic computation.

In order to develop the equations necessary to predict the performance of a freely rotating wheel operating with supersonic axial velocity, it will be assumed that the wheel is operating in a straight annular

duct having purely axial flow with constant total pressure and temperature. For the uniform inflow conditions assumed, the rotor blades generate a negative lift force of such magnitude that its tangential component is equal and opposite to tangential component of the drag (fig. 1), so that the net force on the freely rotating rotor is in the downstream axial direction.

Downstream flow conditions.- The downstream flow conditions as a function of the axial blade force can be computed based upon a one-dimensional analysis involving the solution of the equations of state, conservation of mass, momentum, and energy. With given inflow conditions, all rotor exit conditions are calculable if any two exit parameters can be determined. In the present case, the exit Mach number and stagnation-pressure recovery are the primary dependent variables from which the remaining parameters may be easily found from tables such as those given in reference 15. The solution is given in appendix A and the resulting equations for exit Mach number and stagnation-pressure recovery are

$$M_2 = \left[-\frac{1}{\gamma - 1} - \frac{1}{\gamma(\gamma - 1)(B - 1)} \left(1 - B\sqrt{\gamma^2 - \frac{\gamma^2 - 1}{B}}\right) \right]^{1/2} \tag{1}$$

where

$$B = \frac{\left(M_1^2 + \frac{1}{\gamma} - C_F\right)^2}{M_1^2\left(M_1^2 + \frac{2}{\gamma - 1}\right)}$$

with the axial-force coefficient C_F positive in the direction of air flow and

$$\frac{p_{t,2}}{p_{t,1}} = \frac{M_1}{M_2}\left(\frac{\frac{2}{\gamma - 1} + M_2^2}{\frac{2}{\gamma - 1} + M_1^2}\right)^{\frac{\gamma+1}{2(\gamma-1)}} \tag{2}$$

The variations of exit Mach number and stagnation-pressure recovery as a function of axial-force coefficient for the supersonic range of inlet Mach numbers are presented in figures 2 and 3. In general, there are two values of exit Mach number for any given inlet Mach number; one is supersonic, the other, subsonic. When the axial-force coefficient is zero, that is, there is no rotor, the equations for Mach number and pressure recovery reduce identically to the Rankine-Hugoniot expression for a normal shock, with the lower branch of the curves in figures 2 and 3 representing the conditions behind a normal shock in a supersonic flow

at a Mach number of M_1. Similarly, with a rotor the upper branch of each curve represents the retarding effect due to the blade force alone, whereas the lower branch includes the effect of the downstream normal shock. In the latter case, the pressure recovery is always less than, and the exit Mach number is greater than, that due to the normal shock in a duct without the rotor. For any given axial-force coefficient, there is a minimum inlet Mach number below which no real solution exists. This minimum occurs when the exit Mach number is 1.0.

Axial-force coefficient.- The one-dimensional momentum concept cannot disclose the detailed flow pattern which generates the forces on the blade. For example, for a given axial-force coefficient, the position of the normal shock either upstream or downstream of the rotor is immaterial according to the previous analysis. However, the axial blade force can intuitively be said to be a function of mode of operation. As yet, a theory to predict the performance of a transonic cascade is nonexistent. For this reason, the normal shock will be assumed to be located downstream of the rotor to permit calculation of the blade force in an entirely supersonic stream.

The aerodynamic force reacting upon the blade may be calculated by the linearized supersonic airfoil theory provided that interference effects between blades in cascade are avoided. That is, the trailing edge of any blade is upstream of the wave pattern generated by the adjacent blades. The necessary conditions to insure such operation are investigated subsequently. For the present, it will be assumed that the solidity is sufficiently low so that interference between blades does not exist. The equations for the angle of attack at equilibrium operating speed and the axial-force coefficient are derived in appendix B and are

$$ \alpha = \frac{180}{2\pi}\left[-\cot\beta \pm \sqrt{\cot^2\beta - \left(2C_F + C_{D,o}\right)\sqrt{\left(\frac{M_a}{\cos\beta}\right)^2 - 1}}\,\right] \qquad (3) $$

where the positive value of the radical is used in order to obtain the only physically stable operating value for a given cascade, and

$$ C_F = \frac{\sigma C_D M_a^2}{2\cos^3\beta} = \frac{\sigma C_D M_a^2}{2\sin^3(\phi - \alpha)} \qquad (4) $$

Figure 4 shows the variation of angle of attack as a function of air inlet angle, inlet axial Mach number, and thickness-chord ratio for a diamond profile with an assumed flat-plate friction coefficient of 0.003. It can be seen that the angle of attack remains less than 1° for inlet air angles up to 50°. The effect of the variation of thickness-chord

ratio on angle of attack is much greater than that due to variation of inlet axial Mach numbers.

Blade-setting angle and solidity.- The axial-force coefficient is a function of cascade geometry and operating conditions as shown in equation (4). Although the choice of blade-setting angle ϕ and solidity σ appears to be arbitrary, there are practical limitations in their selection. The lower limit of blade-setting angle is dictated by structural considerations based upon desired maximum blade speed. For particular configurations, the choice of blade-setting angle may be determined for maximum pressure recovery as shown subsequently. The stagnation-pressure recovery varies inversely with solidity so that it would appear that low solidity is desirable from the standpoint of high pressure recovery. On the other hand, it can be intuitively argued that high solidity appears to be necessary for maximum flow-distortion elimination. However, the analysis presented in reference 16 indicates that for constant angle of attack, the lift coefficient remains unchanged with increasing solidity until the leading-edge shock just hits the succeeding blade. With a further increase in solidity, the lift coefficient decreases and becomes zero when the reflecting shock hits the blade from which it was generated. Increasing the solidity beyond this point causes the lift coefficient to oscillate between zero and a successively decreasing maximum value. Therefore, it appears that the solidity desirable for operation in a distorted flow is the maximum solidity for noninterference between blades σ_m which is given in reference 16 as

$$\sigma_m = \frac{\sin[\phi - (\epsilon + \alpha)]}{\sin(\epsilon + \alpha)} \tag{5}$$

(Symbols have been changed to agree with those used in the present paper. The shock-wave angle rather than the Mach angle is used since finite-thickness blades are considered herein.) Since the angle of attack for equilibrium operating conditions has been shown to be very small (fig. 4), for most cases α can be neglected and equation (5) can be reduced to

$$\sigma_m = \frac{\sin(\phi - \epsilon)}{\sin \epsilon} \tag{5a}$$

For the case of maximum solidity for noninterference between blades, an illustrative example of the range of values of C_F is shown in figure 5 for diamond profiles with an assumed value of $C_f = 0.003$. The stagnation-pressure recovery for the same conditions is shown in figure 6. For the range of inlet axial Mach number and thickness-chord ratio investigated, the total-pressure-recovery curves reach a maximum at air inlet angles between 15° and 35°. Therefore, an optimum blade-setting angle for maximum recovery exists for any given condition in undistorted flow. The

fact that peak pressure recoveries occur at air inlet angles less than 35° for all cases considered is advantageous from the structural and weight standpoint for the rotor since wheel speed varies directly with air inlet angle. The total-pressure recovery at peak conditions is approximately 99 percent.

A supersonic, freely rotating rotor with the maximum effective solidity operating at the face of a conical inlet in an undistorted flow will produce a total-pressure loss of 1 percent or less. The ability of such a device to eliminate distortion must be subjected to an experimental investigation.

EXPERIMENTAL INVESTIGATION

Rotor Design

A straight annulus is probably the easiest method of obtaining the completely uniform flow which is required in order to verify experimentally the low losses of a freely rotating blade row predicted in the foregoing analysis. This configuration would necessitate imposing arbitrary distortions in the flow in order to determine the effectiveness of the freely rotating rotor in reducing distortion and the losses incurred with the device operating in distorted flow. Since the use of the proposed device is restricted to conical-type inlets because of the geometry involved, it was felt that the use of a rotor in conjunction with a conical inlet was the best method of determining the overall performance of the device. The distortions produced when the inlet is operating at 0° angle of attack would be negligible or small enough to compare the penalty in measured total-pressure loss with that predicted for undistorted flow; the realistic distortions produced when the inlet is operating at other angles of attack would yield quantitative results on the effectiveness of the device in reducing distortions.

The rotor was designed to operate in conjunction with an existing cowl in an open jet at a Mach number of 2.1. A conical center body having a 25° semivertex angle was chosen to match the cowl-lip angle and to provide an axial Mach number above 1.3 at the rotor inlet so that linearized airfoil theory would apply. A tip speed of 600 ft/sec based upon rotor inlet diameter was arbitrarily selected for a stagnation temperature of 100° F. These conditions determined the velocity diagrams for the three design radial stations. The corresponding inlet flow parameters are tabulated as follows:

Station	r_1	$M_{a,1}$	β_1	M_1
Tip	0.0908	1.55	22.3	1.67
Mean	.0695	1.44	18.3	1.52
Hub	.0476	1.34	13.6	1.38

The airfoil section chosen had a 5-percent thickness-chord ratio and symmetrical flat sides with a 12° included wedge angle at the leading and trailing edges. The solidity at the hub section was chosen equal to the maximum solidity for noninterference between blades which was 0.55.

For structural rigidity and to simplify fabrication, the rotor was constructed with three constant-chord blades. The resulting chord and blade thicknesses were 0.65 and 0.032 inch, respectively.

To insure starting, the rotor was "dished out" as shown in figure 7 by an amount equal to the cross-sectional area of the blades and the center-body shape was adjusted so that the flow area continuously increased from the cowl lip to the simulated combustion chamber. Fairing the center body between the conical nose and the afterbody increased the blade span at the leading edge of the rotor. This resulted in a rotor having an inlet tip diameter of 2.18 inches with a ratio of hub radius to tip radius of 0.52 and an exit tip diameter of 2.43 inches with a ratio of hub radius to tip radius of 0.66. A photograph of the rotor appears in figure 8. In addition, fairing the center body also increased the Mach number near the hub, but this effect was neglected in the design of the rotor.

APPARATUS

Tests of a conical inlet having a 25° semivertex cone angle with and without a freely rotating rotor were performed with low-humidity air in a 9- by 9-inch blowdown jet at a test Mach number of 2.1.

Except for the center body, the experimental model is the same one described in reference 17. A schematic diagram of the test setup showing the conical inlet without the rotor is reproduced in figure 9 and the front portion showing the cowling and center body with the rotor is presented in figure 7. The same center body with interchangeable nose pieces, one with the rotor and one without the rotor, was used. The center body and plain nose piece were constructed with stainless-steel cores and plastic shells forming the outer contours. The nose piece incorporating the rotor was constructed from 17-4 PH stainless steel.

The blades with integral shanks were push fitted into the nose piece and locked in place by peening. The tip clearance under static conditions was 0.016 inch. The cowling which is cowling A of reference 17 had a 12.4° internal and 17° external lip angle with a lip thickness of 0.003 inch. Ordinates for the cowling inner surface and center body are given in table I. The center body was positioned so that at 0° angle of attack the conical shock impinged on the cowl lip. A remote-controlled plug valve, the position of which was indicated by means of a Selsyn indicator, permitted variations of the exit nozzle area during a test.

INSTRUMENTATION

The location of the pressure instrumentation can be seen in figures 7 and 9. Four static-pressure taps in the cowl spaced 1/2 inch apart beginning 3/4 inch behind the cowl lip were used to determine the approximate location of the normal shock. Six three-point total-pressure rakes were equally spaced circumferentially 7 inches behind the cowl lip at station 3. Six static-pressure taps were located in the cowl between these rakes at the same axial station. A nine-point total-pressure rake in conjunction with four static-pressure taps equally spaced circumferentially in the inner and outer walls were used to obtain pressure distributions in the simulated chamber (station 4). The rake which could be rotated was held stationary in the vertical plane since calibration tests indicated no measurable variation in total-pressure recovery as a function of rake position. All pressures were recorded simultaneously by photographing a mercury manometer board.

The rotor speed was obtained by a commercial electronic counter which measured the amplified input signal from an electromagnetic pickup actuated by the rotation of the rotor shaft.

Visual observation of the inlet flow phenomena was afforded by means of a conventional schlieren system.

TEST PROCEDURE

Tests were made with and without the rotor at 0° and positive angles of attack of 4°, 6°, and 8°. The flow was started with the plug valve retracted sufficiently to allow the normal shock to move well downstream of the rotor position. For a given setting of the plug valve photographs of the manometer board, schlieren pictures of the inlet flow, and rotational speed of the rotor were obtained. This procedure was repeated as the plug valve was advanced in small increments until subcritical

operation was noted by watching the inlet flow on a continuously illu-
minated schlieren screen as well as the static taps in the cowl over the
rotor. The five positions of the plug valve at which data were taken
were identical for each test. All tests were made at a stagnation pres-
sure and temperature of 60 lb/sq in. and 100° F, respectively.

PRESENTATION OF DATA

Circumferential and radial distributions and distortions of total
pressure and Mach number at station 3 are presented as a function of
pressure recovery at the simulated combustion chamber for each angle of
attack. The Mach number at each measuring position behind the rotor was
obtained by assuming a constant radial static pressure at each circum-
ferential rake location and using the average of the two cowl static
taps adjacent to each total-pressure rake. The average total-pressure
recovery is the ratio of the arithmetical-average total pressure at
station 3 or station 4 to the settling-chamber stagnation pressure.

The distortions at station 3 are computed in several ways: the
overall distortion is the ratio of the difference between the maximum
and minimum of all values to the arithmetical average of all values;
the circumferential distortion is the ratio of the difference between
the maximum and minimum values for each radial position to the arithmet-
ical average value of all points in the annulus. In addition, an aver-
age circumferential distortion herein called an average for annulus, is
obtained by numerically averaging the circumferential distortions at the
three radial stations. The radial distortion is the ratio of the differ-
ence between the maximum and minimum values for each circumferential
position to the arithmetical average value of all points in the annulus.

RESULTS AND DISCUSSION

Circumferential total-pressure distortion.- The effect of the freely
rotating rotor on circumferential inlet total-pressure distortion is
presented in figures 10 and 11. The benefit obtained from the freely
rotating wheel in reducing inlet distortion is clearly indicated in
figure 10 which is a plot of the total-pressure distortion with the rotor
as a function of the total-pressure distortion without the rotor at each
radial measuring position as well as the average for the annulus for all
angles of attack and back pressures at which tests were made. It can be
seen that for all cases, except for a few points at 0° angle of attack,
all points lie above the 45° line indicating a reduction in distortion
due to the presence of the rotor. Actually, at 0° angle of attack, the

rotor is expected to have very little, if any, effect on inlet distortion because the level of distortion is low. Without the rotor, the inlet total-pressure distortion increased from about 0.1 to 0.3 as the angle of attack was increased from 4° to 8°. At these angles of attack, the freely rotating wheel decreased the distortion by approximately 30 percent.

The inlet circumferential total-pressure distortion is replotted in figure 11 as a function of angle of attack and average total-pressure recovery at the simulated combustion chamber to present the distortion on the basis of inlet operating conditions. These conditions of increasing back pressure from minimum to maximum are labeled in alphabetical sequence. In general, a greater reduction in circumferential distortion was produced by the rotor at the lower back pressures, points A and B, than at the inlet peak pressure recovery, points C and D. This reduction might be expected since the original distortion level without the rotor decreased with increasing back pressure.

Total-pressure recovery.- The circumferential distribution of total-pressure recovery measured at station 3 as a function of angle of attack and total-pressure recovery is shown in figure 12. The three operating conditions presented are minimum back pressure, point A, back pressure for peak inlet pressure recovery, points C or D, and maximum back pressure, point E, as indicated in figure 11. For the sake of clarity the ordinate scales are displaced for each operating condition. It is apparent that the reduction in the distortion level is generally a result of reducing the maximum and raising the minimum value of pressure recovery at any radial station, which is in agreement with the principle of operation of a freely rotating rotor. At maximum back pressure for all angles of attack, the measured pressure recovery in the presence of the rotor is everywhere equal to or greater than that without the rotor; however, inlet buzz occurred at these points and therefore no importance should be attached to these apparent gains in pressure recovery because operation at this condition is undesirable.

The average total-pressure recovery at station 3 with the rotor is compared to that without the rotor in figure 13. For supercritical operation where the normal shock is located between the rotor and station 3 (generally points A to C) the pressure recovery is expected to be identically the same with the rotor as without the rotor as shown in figure 13. This is due to the fact that the throttle positions were identical for both conditions and any loss introduced by the rotor must be eliminated by the normal shock repositioning itself so that the choked nozzle can discharge identical mass flows in either case.

One of the primary purposes of the experimental program was to verify that the loss in total pressure across the rotor was less than 1 percent as predicted by the simplified analysis in the first part of this

paper. Because the total-pressure distribution immediately downstream of the rotor could not be measured because of the possibility of the presence of the pressure probes choking the inlet, the rotor total-pressure loss must be inferred from the pressure recovery measured at station 3. This can be done only at peak pressure recovery since shock movement at this point can no longer compensate for any rotor losses. Since the peak pressure recovery occurred at the critical operating point, this condition at 0° angle of attack most nearly duplicates the assumption of supersonic distortion-free inflow to the rotor. The prediction of less than 1 percent loss in total pressure across the rotor is substantiated in figure 13(a) which shows no difference within experimental accuracy between the total-pressure recovery measured with and without the rotor at the peak-pressure-recovery point. The method of determining rotor total-pressure loss might be rejected on the basis that the pressure was measured about $6\frac{1}{4}$ inches behind the rotor and,

therefore, the pressure recovery of the rotor is not actually known. However, if the rotor produced any loss it was washed out by the increased pressure recovery for the duct between the rotor and the measuring rakes as a consequence of the more uniform flow produced by the rotor. Hence, the net result of the effect of the rotor on the inlet would be the same, that is, no pressure loss. This reasoning is strengthened by the fact that at high angles of attack, where the distortion increased, results at station 3 with the rotor show the same average total-pressure recoveries within experimental accuracy as were obtained without the rotor. Actually, the rotor losses would be expected to be higher in distorted flow and increase with increasing distortion. In addition, the freely rotating wheel cannot add any net energy to the flow. Therefore, the fact that the maximum pressure recovery was unaffected by the presence of the rotor must be attributed to the lower duct losses between the rotor exit plane and station 3.

The effect of the freely rotating rotor on the average total-pressure recovery for the entire supersonic inlet (from the intake to the simulated combustion chamber) can be observed in figure 11. At 0° and 4° angle of attack there is no measurable difference in the peak values of inlet total-pressure recovery with and without the rotor. However, at 6° and 8° angle of attack, increases of $1\frac{1}{2}$ and $3\frac{1}{2}$ percent,

respectively, in peak inlet pressure recovery were obtained with the rotor. Since the average pressure recoveries measured at station 3 for both angles of attack with and without the rotor were within 1 percent of each other (figs. 13(c) and 13(d)), the increase in inlet pressure recovery obtained with the freely rotating wheel must be attributed to lower duct losses between station 3 and the simulated combustion chamber as a consequence of the more uniform flow created by the rotor. Apparently, placing the rotor at the cowl inlet rather than in the subsonic flow field near the compressor face increases its total benefit because

of the ability of the diffuser to more than make up any losses incurred by the rotor.

Circumferential Mach number distortion.- The ability of a multistage axial-flow compressor to operate in a distorted flow without surging is primarily dependent upon the inlet velocity distortion rather than upon total-pressure distortion. Since no attempt was made to measure the temperature behind the rotor, the actual velocity distribution is not known. However, because the total-pressure rise or drop at any position is small, the stagnation temperature distribution can be assumed to be uniform. Therefore, for the measured range of Mach number at station 3 the velocity distortion is approximately equal to the Mach number distortion. To calculate the Mach number the radial static pressure was assumed to be constant. The validity of this assumption is shown by the results presented in reference 18 in which it was shown that, for a similar inlet, small radial static-pressure variations exist when the circumferential variations are small. In the present investigation the average circumferential cowl static-pressure variation measured at station 3 was 1.3 percent without the rotor and 0.9 percent with the rotor.

The effect of the freely rotating rotor on the circumferential Mach number distortion is presented in figures 14 and 15. The overall ability of the freely rotating wheel to reduce the Mach number distortion can be seen in figure 14 which is a plot of the circumferential Mach number distortion with the rotor as a function of the Mach number distortion without the rotor at each radial measuring station as well as the average for the annulus for all angles of attack and back pressures tested. At 0° angle of attack the rotor had essentially no effect on the average Mach number distortion of about 0.15 which was present without the rotor. The circumferential Mach number distortion without the rotor increased from about 0.4 to 1.3 as the angle of attack was increased from 4° to 8°. The freely rotating rotor reduced this distortion by approximately 25 percent.

In order to show the effect of inlet operating conditions on the Mach number distortion with and without the freely rotating rotor, the circumferential Mach number distortion is plotted in figure 15 as a function of angle of attack and average total-pressure recovery at the simulated combustion chamber. The conditions of increasing back pressure are again labeled in alphabetical sequence. The circumferential Mach number distortion decreased with increasing back pressure with and without the rotor and a greater reduction of this distortion was obtained with the rotor at the lower back pressures. These results are similar to the results obtained for the total-pressure distortion and are expected since in the absence of a static-pressure distortion, the total-pressure distortion is, in effect, a velocity or Mach number distortion.

Circumferential distribution of Mach number.- The circumferential distribution of Mach number measured at station 3 as a function of angle of attack and back pressure is shown in figure 16. The same three operating conditions as given for the distributions of total-pressure ratio in figure 13 were chosen and the ordinate scales are displaced for clarity. Although the freely rotating rotor generally decreased the Mach number level near the tip and increased the Mach number level near the hub, it had practically no effect on the average Mach number levels for all angles of attack and back pressures tested. At the minimum back pressure the average Mach number was 0.4 while at the two higher back pressures the average Mach number was 0.3'.

Radial distortion.- The effect of the freely rotating rotor on radial inlet total-pressure distortion and on Mach number distortion as functions of angle of attack and back pressure is presented in figures 17 and 18, respectively. Because measurements were made at only three radial positions, these results cannot be considered conclusive but they do show that the radial distortions were generally reduced by the rotor. The radial total-pressure distortions (fig. 17) without the rotor were no greater than 10 percent at any operating condition. For angles of attack of 0° to 6° the greatest reduction in total-pressure distortion occurs at minimum back pressure where the distortion level is highest. On the other hand, at 8° angle of attack the rotor is more effective in reducing distortions at the higher back pressures. It is apparent that the higher the initial radial total-pressure distortion (about 0.1), the greater the reduction of distortion (about 0.3) due to the presence of the rotor. For initial radial total-pressure distortions of 0.05 or less, no effective changes are noted. The radial Mach number distortions presented in figure 18 exhibit trends similar to those shown by the radial total-pressure distortions. The maximum radial Mach number distortion was about 0.4. Apparently, for this conical inlet the radial distortions are significantly smaller than the circumferential distortions.

Overall distortion.- The overall annular total-pressure and Mach number distortions at station 3 are presented in figure 19 in which the distortion with the rotor is plotted as a function of the distortion without the rotor for all operating conditions. The total-pressure distortion without the rotor increased from about 0.1 to 0.4 as the angle of attack increased to 8° (fig. 19(a)). The average reduction in the annular distortion due to the rotor was about 30 percent. The initial Mach number distortion (fig. 19(b)) varied from about 0.4 to 1.4 over the range of angle of attack. The rotor reduced this distortion an average of 23 percent.

Rotor operation.- An indication of how closely the rotor approached its design operating condition can be determined from the measured rotational speed. The flow field at the leading edge of the rotor is not

completely conical because the curvature of the faired portion of the center body upstream of the rotor creates local acceleration of the flow near the rotor hub. However, because the rotor with the inlet operating at 0° angle of attack attained 99 percent of the design rotational speed, the effect of the curvature on the rotor operation is apparently negligible.

At 0° angle of attack the rotor tip speed of 595 ft/sec was constant with increasing back pressure until the maximum back pressure was obtained at which point inlet buzz occurred and the rotor tip speed decreased to 423 ft/sec. With increasing angle of attack, the rotor speed of minimum back pressure decreased to 523 ft/sec at 8° angle of attack. The back pressure at which the speed decreased was progressively lower with increasing angle of attack and was considerably less than that necessary to cause inlet buzz.

CONCLUSIONS

An investigation has been made on the use of a freely rotating rotor at the cowl face of a supersonic conical diffuser to determine its effectiveness in reducing inlet flow distortion and the penalty in terms of total-pressure loss imposed by such a device when distortions are negligible. Tests were made with a rotor having an inlet tip diameter of 2.18 inches and a ratio of hub radius to tip radius of 0.52 in conjunction with a conical inlet having a 25° semivertex cone angle at a Mach number of 2.1 over an angle-of-attack range of 0° to 8°. The following conclusions are drawn:

1. An analysis in which simplified criteria and two-dimensional linearized airfoil theory are used shows that a freely rotating rotor with maximum solidity for noninterference between blades can be designed to operate in an undistorted flow with a total-pressure loss of less than 1 percent.

2. With the inlet operating at 0° angle of attack, the experimental freely rotating rotor produced no measurable total-pressure loss. In addition, at all higher angles of attack where increased rotor losses may be expected, the total peak pressure recovery was the same within experimental accuracy as that obtained without the rotor.

3. The rotor increased the peak total-pressure recovery at the simulated combustion chamber $1\frac{1}{2}$ and $3\frac{1}{2}$ percent at 6° and 8° angle of attack, respectively. This increase is attributed to lower diffusion duct losses as a consequence of a more uniform flow created by the rotor.

4. The overall total-pressure distortions were reduced approximately 30 percent by the presence of the rotor for initial distortions of 0.1 to 0.4 caused by an angle-of-attack increase from 4° to 8°. For the same range of angle of attack, the overall Mach number distortions were reduced approximately 23 percent where the initial distortion ranged from 0.4 to 1.4.

5. In a conical inlet the maximum radial total-pressure and Mach number distortions of about 0.1 and 0.4, respectively, are of minor importance as compared with the maximum circumferential total-pressure and Mach number distortions of about 0.3 and 1.3, respectively.

Langley Research Center,
 National Aeronautics and Space Administration,
  Langley Field, Va., March 5, 1959.

APPENDIX A

EXIT MACH NUMBER AND TOTAL-PRESSURE RECOVERY

AS A FUNCTION OF AXIAL FORCE

In order to determine the exit flow conditions downstream of a freely rotating rotor, a one-dimensional frictionless analysis is used in which the rotor is replaced by an actuator disk across which the flow properties are assumed to vary discontinuously. Attention is focused on an elemental area between two concentric circular cylinders separated a unit distance apart without regard to radial position. Because no torque force can exist, the inlet and exit flow areas must be equal. Therefore, the continuity equation can be written

$$\rho_1 V_1 = \rho_2 V_2 \qquad (A1)$$

Since the only force existing in the plane of the actuator disk must be axial, the equation for the conservation of momentum becomes

$$\rho_1 V_1{}^2 - \rho_2 V_2{}^2 = p_2 - p_1 + (F_a/A) \qquad (A2)$$

where

A   flow area

F_a axial force on the disk, positive in direction of flow and equal and opposite in direction to force reacting on disk

Through the use of the equation of state

$$p = \rho R T \qquad (A3)$$

and the equation for the speed of sound

$$a^2 = \gamma R T \qquad (A4)$$

and the definition of Mach number

$$M = V/a \qquad (A5)$$

equation (A2) can be rewritten as

$$\frac{p_2}{p_1} = \frac{M_1^2 + \frac{1}{\gamma} - \frac{F_1}{\gamma p_1 A}}{\left(\frac{1}{\gamma} + M_2^2\right)} \tag{A6}$$

From equations (A1), (A3), (A4), and (A5)

$$\frac{T_2}{T_1} = \left(\frac{p_2}{p_1}\right)^2 \left(\frac{M_2}{M_1}\right)^2 \tag{A7}$$

The energy equation is

$$\frac{\gamma}{\gamma - 1} \frac{p_1}{\rho_1} + \frac{V_1^2}{2} = \frac{\gamma}{\gamma - 1} \frac{p_2}{\rho_2} + \frac{V_2^2}{2} \tag{A8}$$

Using equations (A3), (A4), and (A5) with equation (A8) results in

$$\frac{T_2}{T_1} = \frac{\frac{2}{\gamma - 1} + M_1^2}{\frac{2}{\gamma - 1} + M_2^2} \tag{A9}$$

Combining equations (A6), (A7), and (A9) gives

$$\frac{M_1^2 \left(\frac{2}{\gamma - 1} + M_1^2\right)}{\left(M_1^2 + \frac{1}{\gamma} - \frac{F_a}{\gamma p_1 A}\right)^2} = \frac{M_2^2 \left(\frac{2}{\gamma - 1} + M_2^2\right)}{\left(M_2^2 + \frac{1}{\gamma}\right)^2} \tag{A10}$$

Solving equation (A10) for M_2 yields

$$M_2 = \left[-\frac{1}{\gamma - 1} - \frac{1}{\gamma(\gamma - 1)(B - 1)}\left(1 \pm B\sqrt{\gamma^2 - \frac{\gamma^2 - 1}{B}}\right) \right]^{1/2} \tag{A11}$$

where

$$B = \frac{\left(M_1^2 + \frac{1}{\gamma} - \frac{F_a}{\gamma p_1 A}\right)^2}{M_1^2 \left(M_1^2 + \frac{2}{\gamma - 1}\right)}$$

Defining an axial-force coefficient per unit area as

$$C_F = \frac{F_a}{n\gamma p_1 G}$$

where $nG = A$ for a unit span, gives

$$B = \frac{\left(M_1{}^2 + \frac{1}{\gamma} - C_F\right)^2}{M_1{}^2\left(M_1{}^2 + \frac{2}{\gamma - 1}\right)}$$

The total-pressure recovery as a function of inlet and exit Mach number can be determined as follows:

$$\frac{p_{t,2}}{p_{t,1}} = \left(\frac{p_{t,2}}{p_2}\right)\left(\frac{p_1}{p_{t,1}}\right)\left(\frac{p_2}{p_1}\right) \tag{A12}$$

Substituting the isentropic-flow relationship between pressure ratio and Mach number

$$\frac{p_t}{p} = \left(1 + \frac{\gamma - 1}{2} M^2\right)^{\frac{\gamma}{\gamma-1}}$$

and equations (A7) and (A9) in equation (A12) results in

$$\frac{p_{t,2}}{p_{t,1}} = \frac{M_1}{M_2}\left(\frac{\frac{2}{\gamma - 1} + M_2{}^2}{\frac{2}{\gamma - 1} + M_1{}^2}\right)^{\frac{\gamma+1}{2(\gamma-1)}} \tag{A13}$$

Equation (A13) may be evaluated through the use of tabulated functions in reference 15 since

$$\frac{M_1}{M_2}\left(\frac{\frac{2}{\gamma - 1} + M_2{}^2}{\frac{2}{\gamma - 1} + M_1{}^2}\right)^{\frac{\gamma+1}{2(\gamma-1)}} = \frac{A_2}{A_1} = \frac{A_2}{A_{cr}} \frac{A_{cr}}{A_1}$$

APPENDIX B

DERIVATION OF EQUATIONS OF OPERATING ANGLE OF ATTACK

AND AXIAL-FORCE COEFFICIENT

The well-known linearized lift and drag coefficients can be written as

$$C_L = \frac{4\pi}{180} \frac{\alpha}{\sqrt{\left(\frac{M_a}{\cos \beta}\right)^2 - 1}} \tag{B1}$$

and

$$C_D = 4\left(\frac{\pi}{180}\right)^2 \frac{\alpha^2}{\sqrt{\left(\frac{M_a}{\cos \beta}\right)^2 - 1}} + 2C_f + C_{D,o} \tag{B2}$$

where $C_{D,o}$ is a function of shape and thickness-chord ratio (ref. 15). The relationship for the diamond profile is

$$C_{D,o} = 4 \frac{(t/c)^2}{\sqrt{\left(\frac{M_a}{\cos \beta}\right)^2 - 1}} \tag{B3}$$

Referring to figure 1, it can be seen that the requirement that the tangential force on the blade vanish at the equilibrium operating speed yields the following Lift/Drag relationship

$$C_L/C_D = -\tan \beta \tag{B4}$$

Substituting equations (B1) and (B2) in equation (B4) and solving for the equilibrium angle of attack yields

$$\alpha = \frac{180}{2\pi}\left[-\cot \beta \pm \sqrt{\cot^2\beta - \left(2C_f + C_{I,o}\right)\sqrt{\left(\frac{M_a}{\cos \beta}\right)^2 - 1}}\right] \tag{B5}$$

where the positive value of the radical is used in order to obtain the only physically stable operating value for a given cascade.

Referring to figure 1, the axial force per blade per unit span is

$$-\frac{F_a}{n} = L \sin \beta - D \cos \beta \qquad (B6)$$

or the axial force per unit disk area is

$$-\frac{F_a}{nG} = \frac{L \sin \beta}{G} - \frac{D \cos \beta}{G} \qquad (B7)$$

Since

$$L = \frac{\gamma p}{2} \frac{M_a^2}{\cos^2 \beta} C_L c$$

$$\frac{c}{G} = \sigma$$

and

$$\frac{C_L}{C_D} = -\tan \beta$$

equation (B7) can be written as

$$C_F = \frac{\sigma C_D M_a^2}{2 \cos^3 \beta} \qquad (B8)$$

or

$$C_F = \frac{\sigma C_D M_a^2}{2 \sin^3(\phi - \alpha)} \qquad (B8a)$$

REFERENCES

1. Conrad, E. William, and Sobelewski, Adam E.: Investigation of Effects of Inlet-Air Velocity Distortion on Ferformance of Turbojet Engine. NACA RM E50G11, 1950.

2. Huntley, S. C., Sivo, Joseph N., and Walter, Curtis L.: Effect of Circumferential Total-Pressure Gradients Typical of Single-Inlet Duct Installations on Performance of an Axial-Flow Turbojet Engine. NACA RM E54K26a, 1955.

3. Conrad, E. William, Hanson, Morgan P., and McAulay, John E.: Effects of Inlet-Air-Flow Distortion on Steady-State Altitude Performance of an Axial-Flow Turbojet Engine. NACA RM E55A04, 1955.

4. Fenn, David B., and Sivo, Joseph N.: Effect of Inlet Flow Distortion on Compressor Stall and Acceleration Characteristics of a J65-B-3 Turbojet Engine. NACA RM E55F20, 1955.

5. Piercy, Thomas G.: Factors Affecting Flow Distortions Produced by Supersonic Inlets. NACA RM E55L19, 1956.

6. Ashby, George C., Jr.: Investigation of the Effect of Velocity Diagram on Inlet Total-Pressure Distortions Through Single-Stage Subsonic Axial-Flow Compressors. NACA RM L57A03, 1957.

7. Smith, L. H., Jr.: Recovery Ratio - A Measure of the Loss Recovery Potential of Compressor Stages. Paper No. 56 - A-206, A.S.M.E. Nov. 1956.

8. Piercy, Thomas G., and Klann, John L.: Experimental Investigation of Methods of Improving Diffuser-Exit Total-Pressure Profiles for a Side-Inlet Model at Mach Number 3.05. NACA RM E55F24, 1955.

9. Farley, John M., and Seashore, Ferris L.: Full-Scale, Free-Jet Investigation of Methods of Improving Outlet Flow Distribution in a Side-Inlet Supersonic Diffuser. NACA RM E54L31a, 1955.

10. Sterbentz, William H.: Factors Controlling Air-Inlet Flow Distortions. NACA RM E56A30, 1956.

11. Collar, A. R.: The Use of a Freely Rotating Windmill To Improve the Flow in a Wind Tunnel. R. & M. No. 1856, British A.R.C., 1939.

12. Johnston, I. H.: The Use of Freely Rotating Blade Rows To Improve Velocity Distribution in an Annulus. National Gas Turbine Establishment Memo. No. M.109, British Ministry of Supply, Feb. 1951.

13. English, Robert E., and Yohner, Peggy L.: Theoretical Analysis of One-Stage Windmills for Reducing Flow Distortion. NACA RM E57D05, 1957.

14. Sanders, Newell D., and Palasics, John: Analysis of Effects of Inlet Pressure Losses on Performance of Axial-Flow Type Turbojet Engine. NACA RM E8J25b, 1948.

15. Ferri, Antonio: Elements of Aerodynamics of Supersonic Flows. The MacMillian Co., 1949.

16. El Badrawy, Rashad M.: Flat Plate Cascades at Supersonic Speed. NACA TM 1369, 1956.

17. Trimpi, Robert L., and Cohen, Nathaniel B.: Effect of Several Modifications to Center Body and Cowling on Subcritical Performance of a Supersonic Inlet at Mach Number of 2.02. NACA RM L55C16, 1955.

18. Piercy, Thomas G., and Chiccine, Bruce G.: Development of Flow Distortions in a Full-Scale Nacelle Inlet at Mach Numbers 0.63 and 1.6 to 2.0. NACA RM E56G13a, 1956.

TABLE I

ORDINATES OF COWLING INNER SURFACE AND CENTER BODY

Cowling		Center body			
X, in.	r_c, in.	x, in.	— r, in.		
			With rotor		Without rotor
0	1.094	0	0		0
.30	1.162	.25	*(Linear variation)*		*(Linear variation)*
.80	1.275	.50			
1.30	1.365	.75			
1.80	1.430	1.000			
2.30	1.485	1.130	.527		.527
2.80	1.530	1.251	.565		.584
3.30	1.560	1.399	.616		.648
4.00	1.580	1.568	.687		.712
-----	*(Linear variation)*	1.737	.756		.770
-----		1.885	.816		.818
-----		1.951	.830		-----
-----		1.981	-----		.840
-----		2.531		0.971	
-----		3.031		1.049	
-----		3.531		1.111	
-----		4.031		1.160	
-----		4.531		1.188	
-----		4.860		1.187	
-----		5.00		1.183	
-----		5.25		1.170	
-----		5.50		1.160	
12.0	1.74	5.75		1.148	
12.5	1.76	6.0		1.136	
13.0	1.77	6.5		1.111	
13.5	1.79	7.5		1.060	
14.0	1.81	8.5		1.008	
14.5	1.82	9.5		.956	
15.0	1.84	10.5		.904	
20.5	2.01	11.5		.851	
47.0	2.01	12.5		.799	
47.5	1.75	13.5		.748	
54.5	1.75	14.5		.696	

Figure 1.- Typical velocity diagram for supersonic cascade of diamond profiles with resulting blade forces and wave pattern.
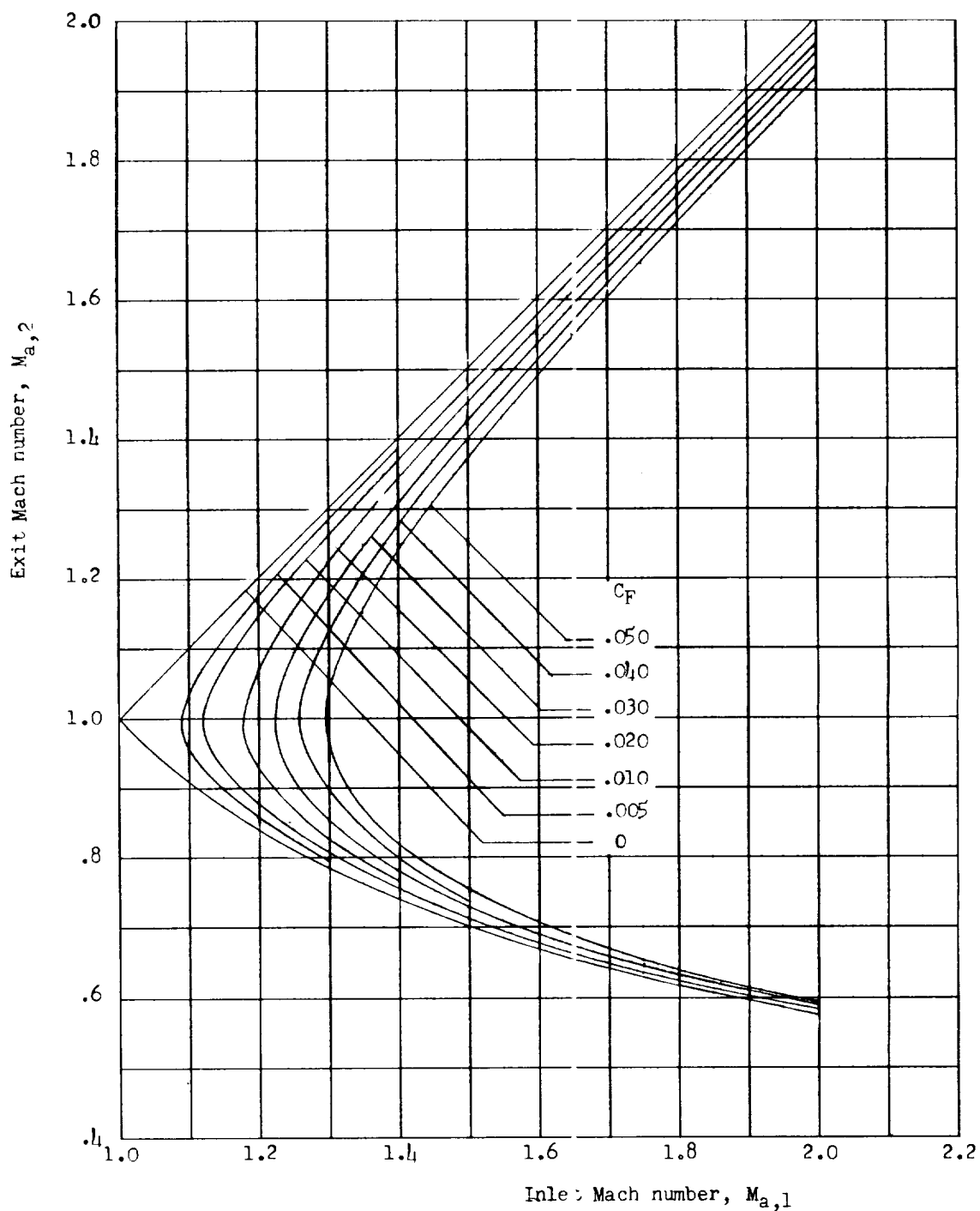
Figure 2.- Variation of exit Mach number with inlet Mach number as a
function of axial-force coefficient.
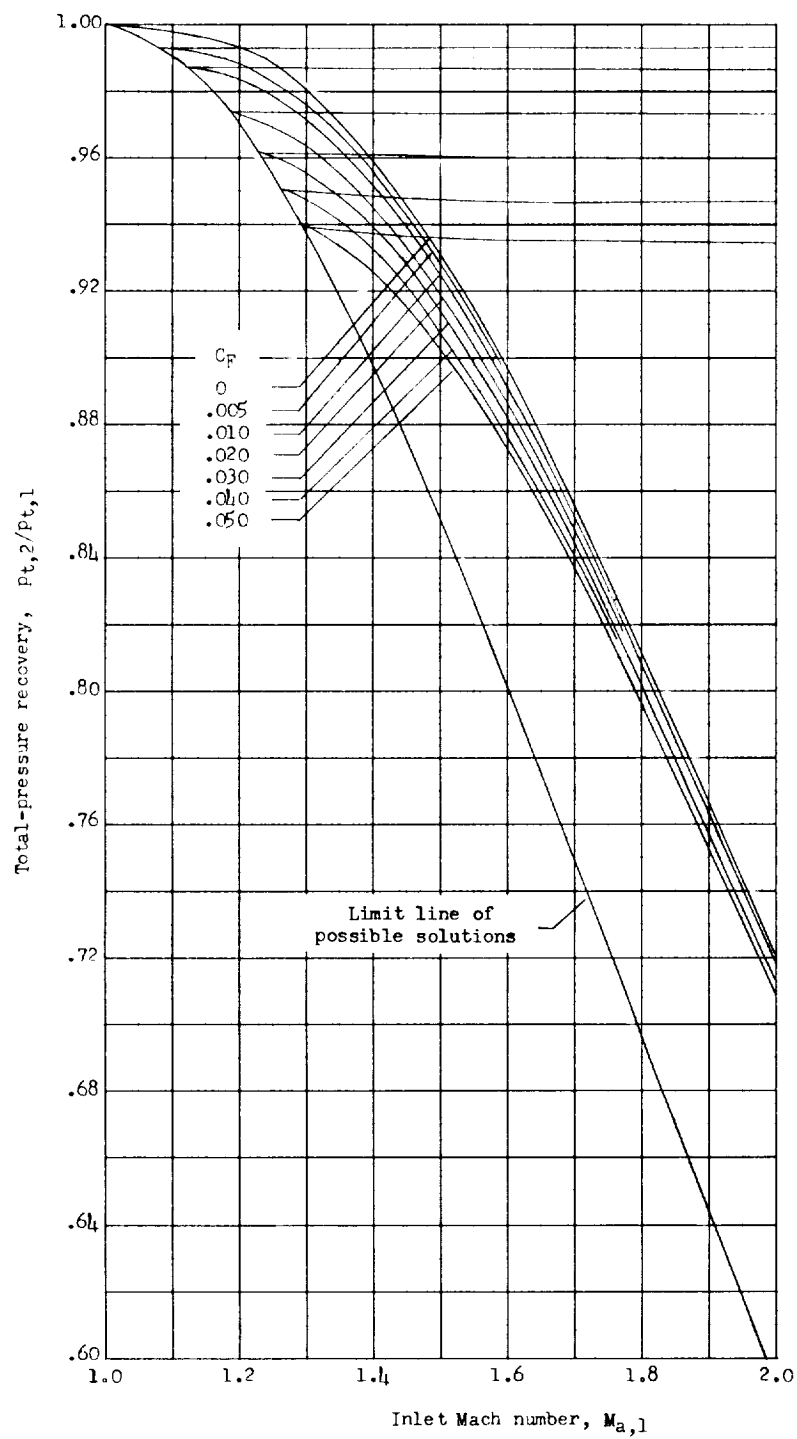
Figure 3.- Variation of total-pressure recovery with inlet Mach number
as a function of axial-force coefficient.
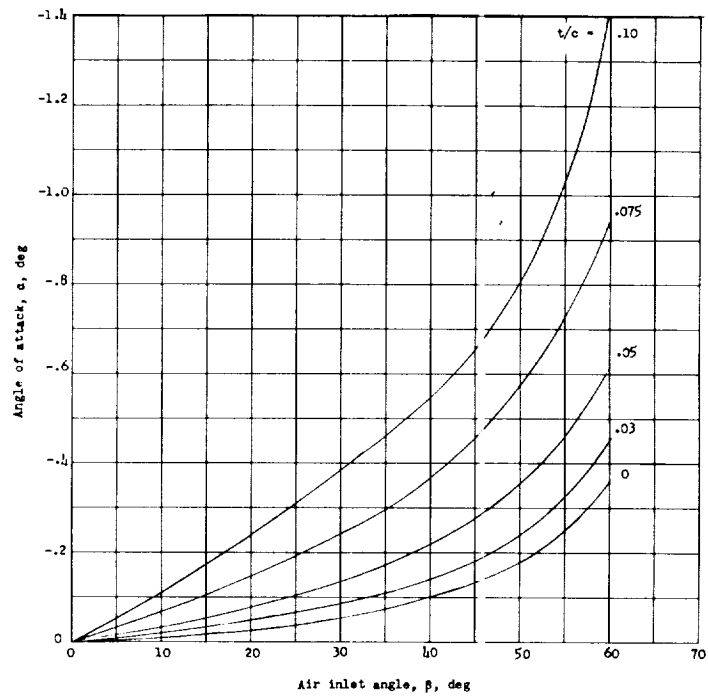
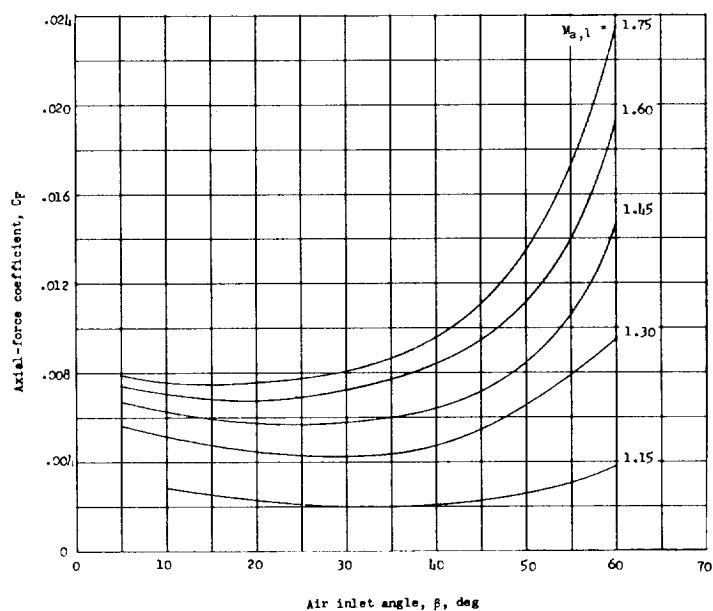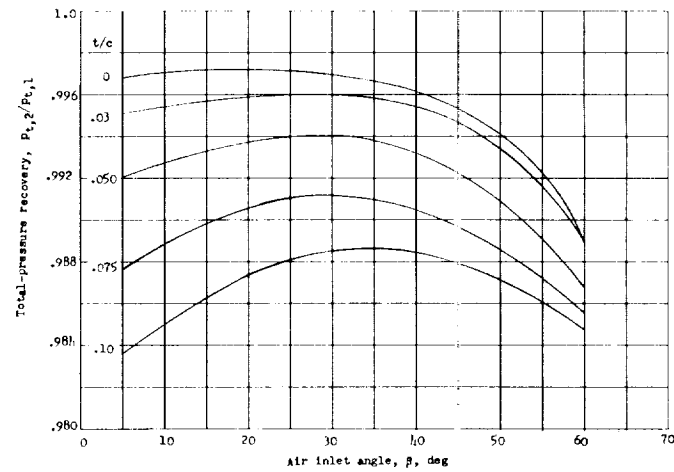(a) Effect of variation of thickness-chord ratio. $M_{a,1} = 1.3$.
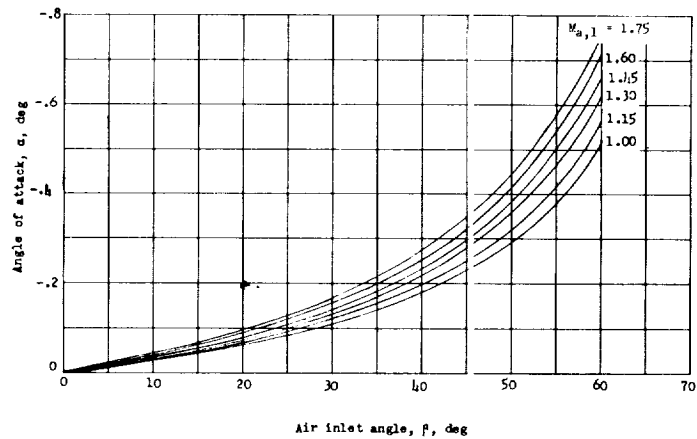
(b) Effect of variation of axial Mach number. $t/c = 0.05$.

Figure 4.- Variation of angle of attack with air inlet angle as a function of thickness-chord ratio and axial Mach number for diamond profile and assumed value of $C_f = 0.003$. No distortion.
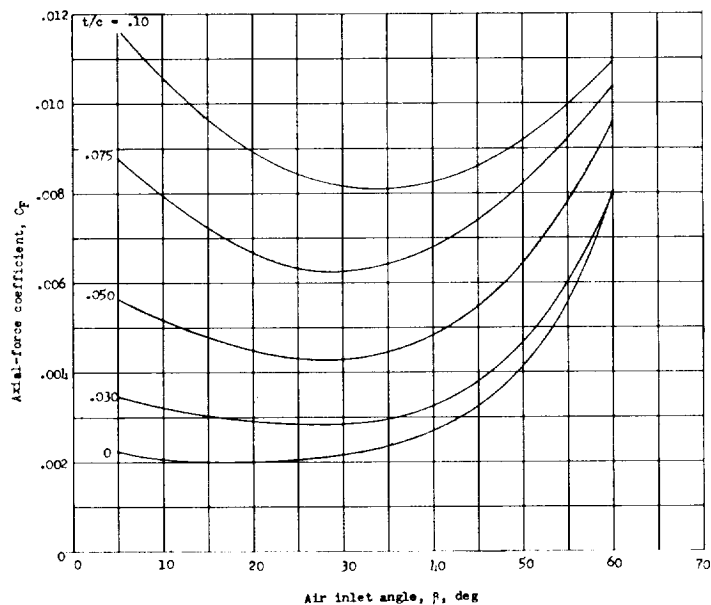
(a) Effect of variation of thickness-chord ratio. $M_{a,1} = 1.3$.

(b) Effect of variation of axial Mach number. $t/c = 0.05$.

Figure 5.- Variation of axial-force coefficient with air inlet angle as a function of thickness-chord ratio and axial Mach number for diamond profiles and assumed value of $C_f = 0.003$. No distortion.

(a) Effect of variation of thickness-chord ratio. $M_{a,1} = 1.3$.
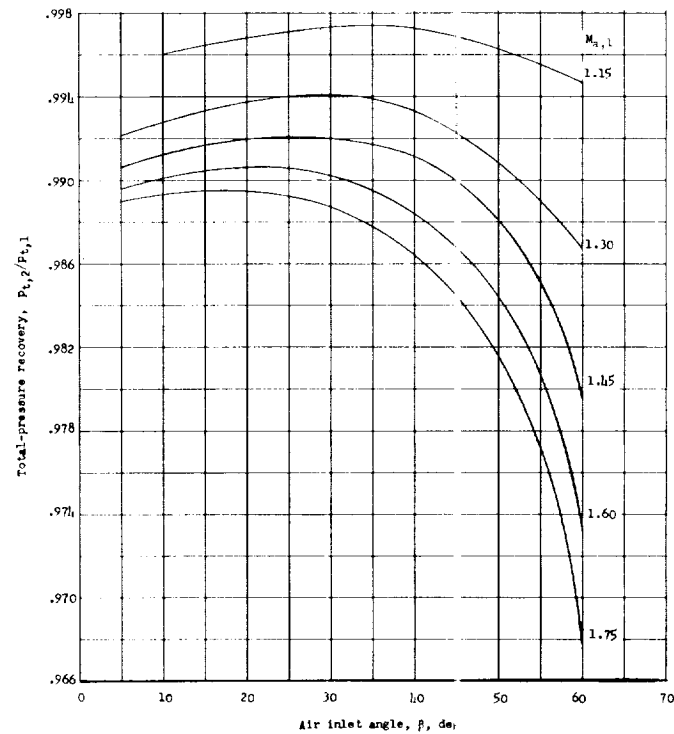
(b) Effect of variation of axial Mach number. $t/c = 0.05$.

Figure 6.- Variation of total-pressure recovery with air inlet angle as a function of thickness-chord ratio and axial Mach number for diamond profile and assumed value of $C_f = 0.003$. No distortion.

Figure 7.- Construction and instrumentation details. Dimensions are in inches.

Figure 8.- Freely rotating rotor. L-57-4359
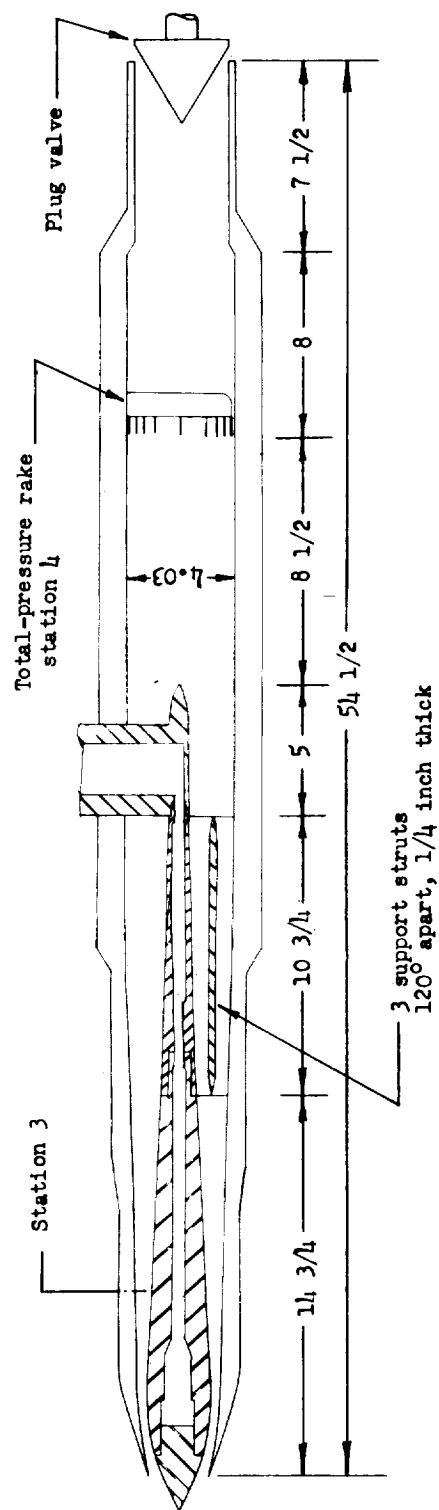
Figure 9.- Schematic diagram of model tested. Dimensions are in inches.

(a) $\dfrac{r_3}{r_{c,3}} = 0.903.$

(b) $\dfrac{r_3}{r_{c,3}} = 0.805.$

Circumferential total-pressure distortion, $\Delta p_t / p_t$, with rotor

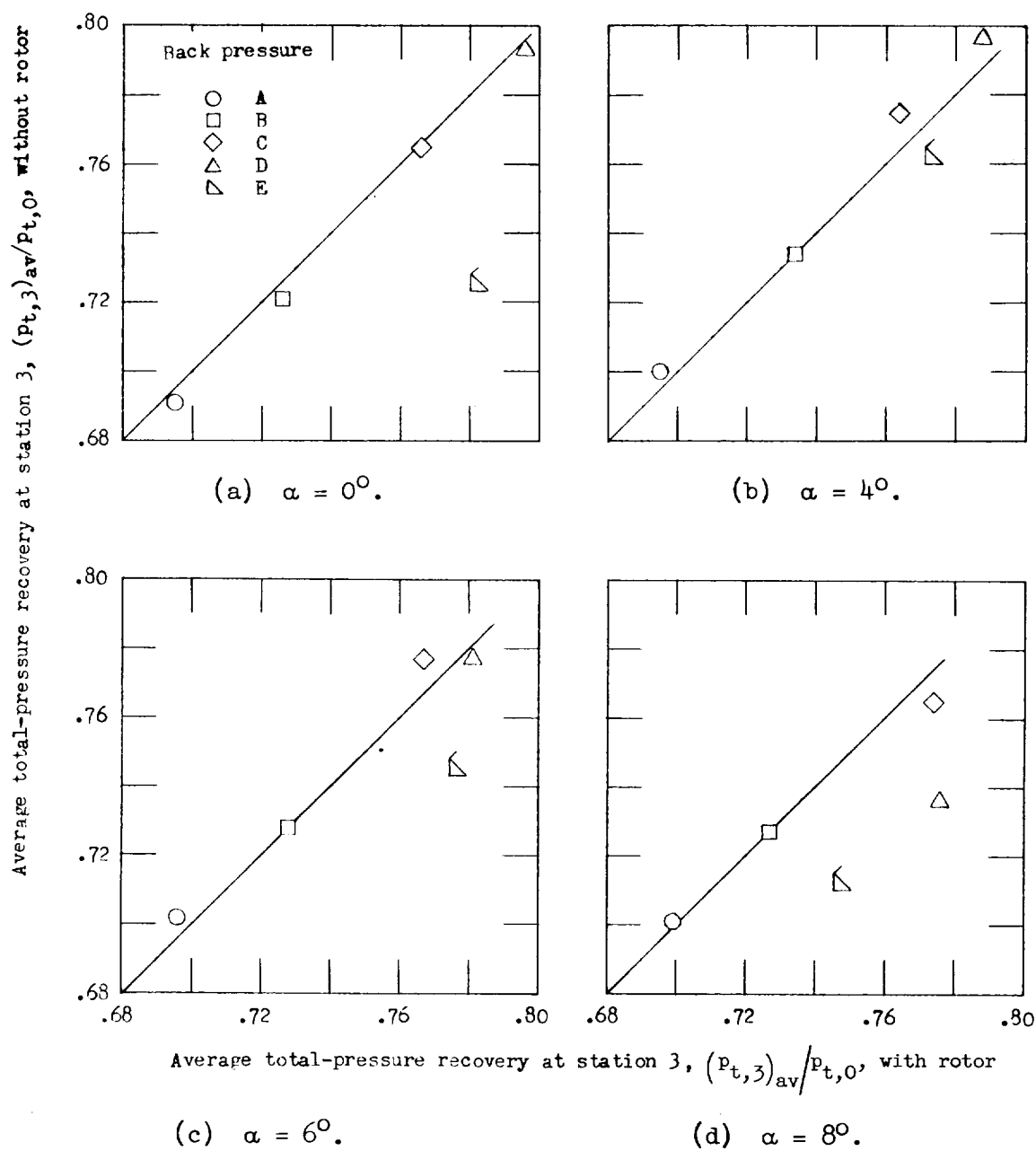(c) $\dfrac{r_3}{r_{c,3}} = 0.707.$ (d) Average for annulus.
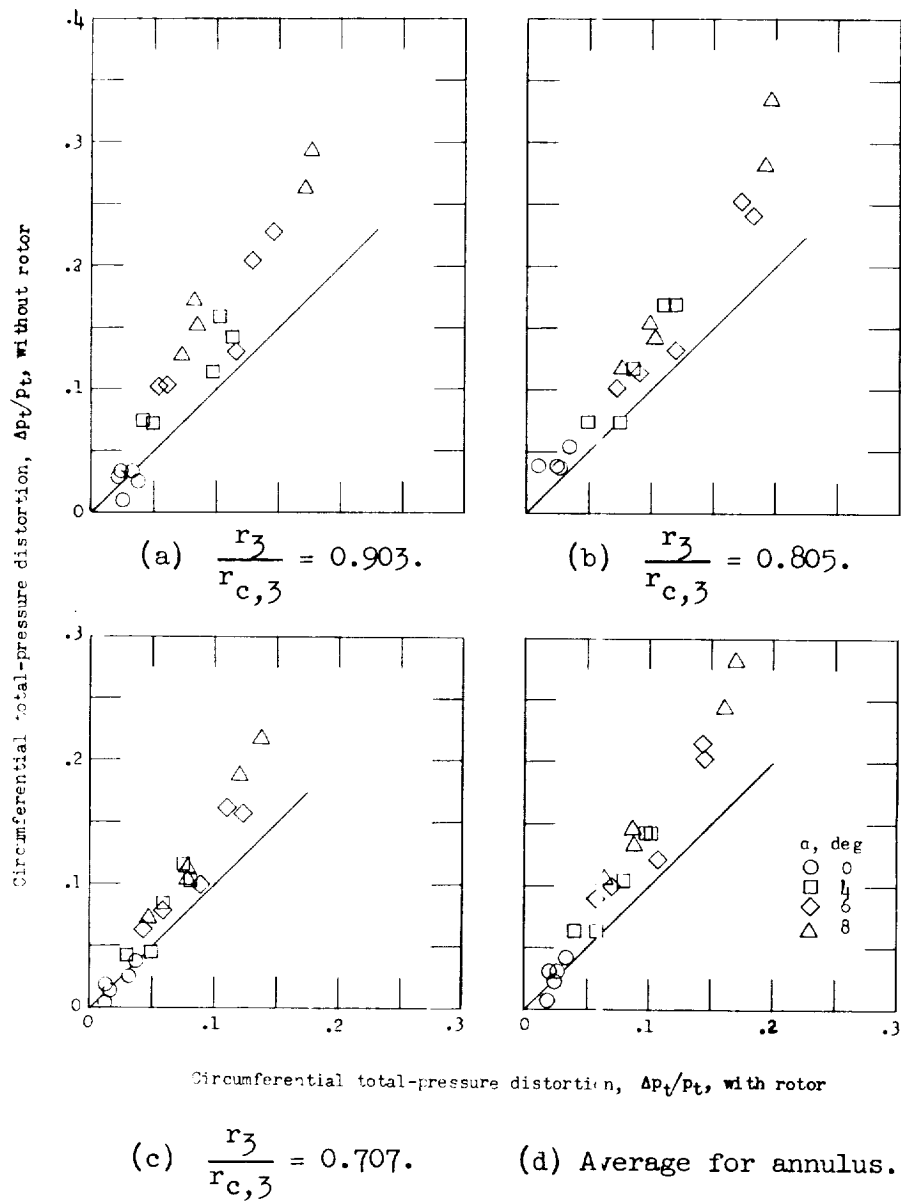
Figure 10.- Circumferential total-pressure distortion with and without freely rotating rotor for all angles of attack and back pressures. Flagged symbols indicate buzz.
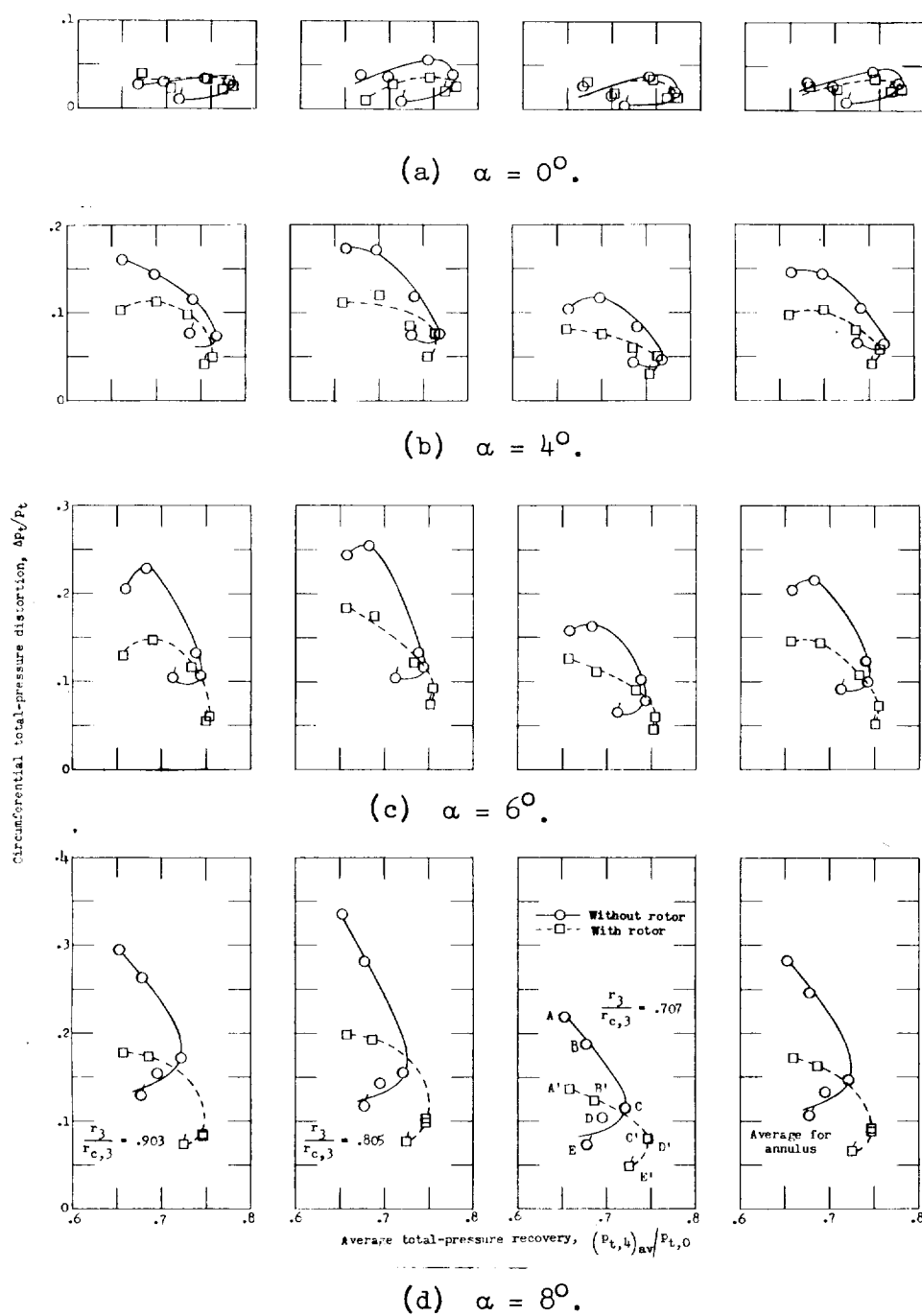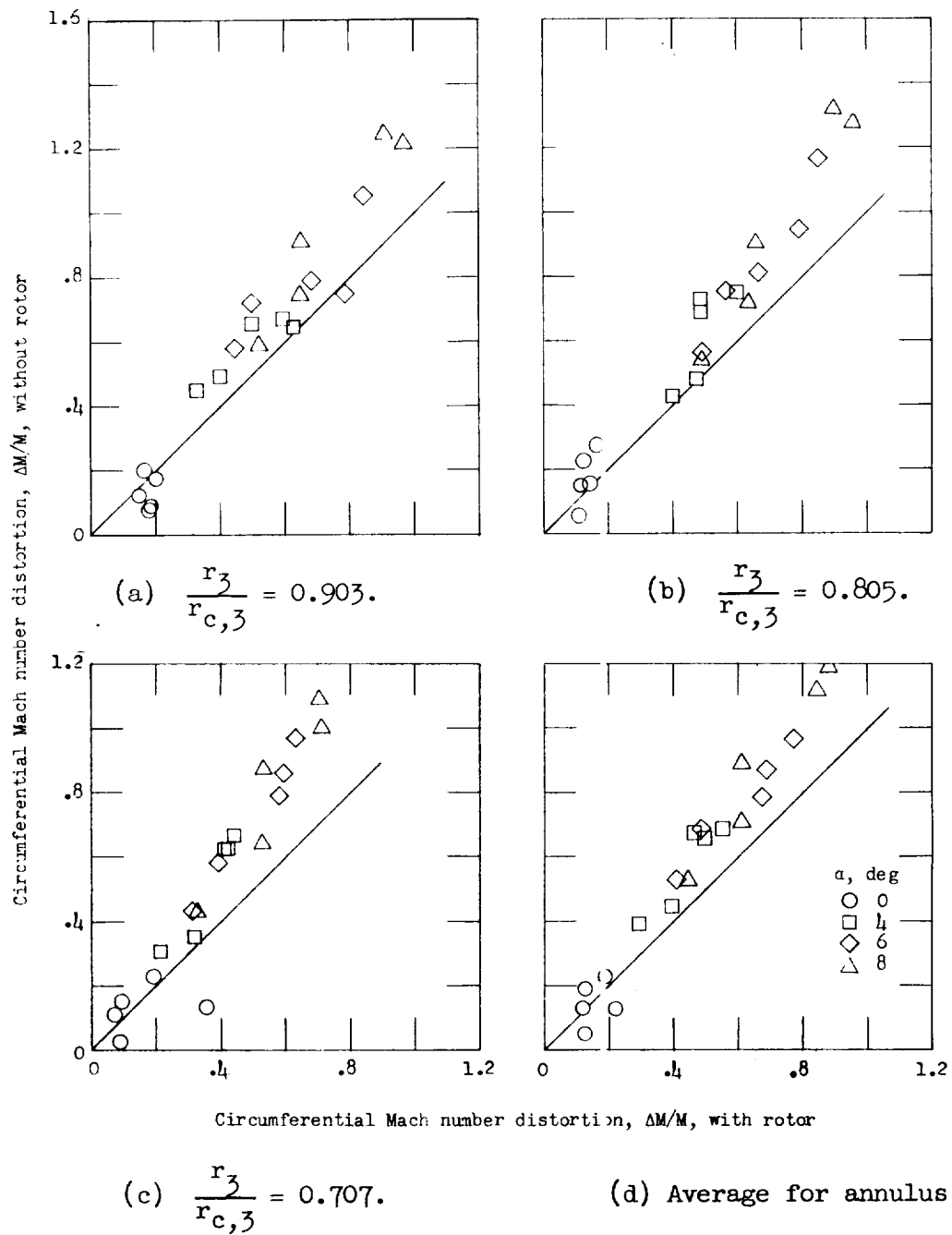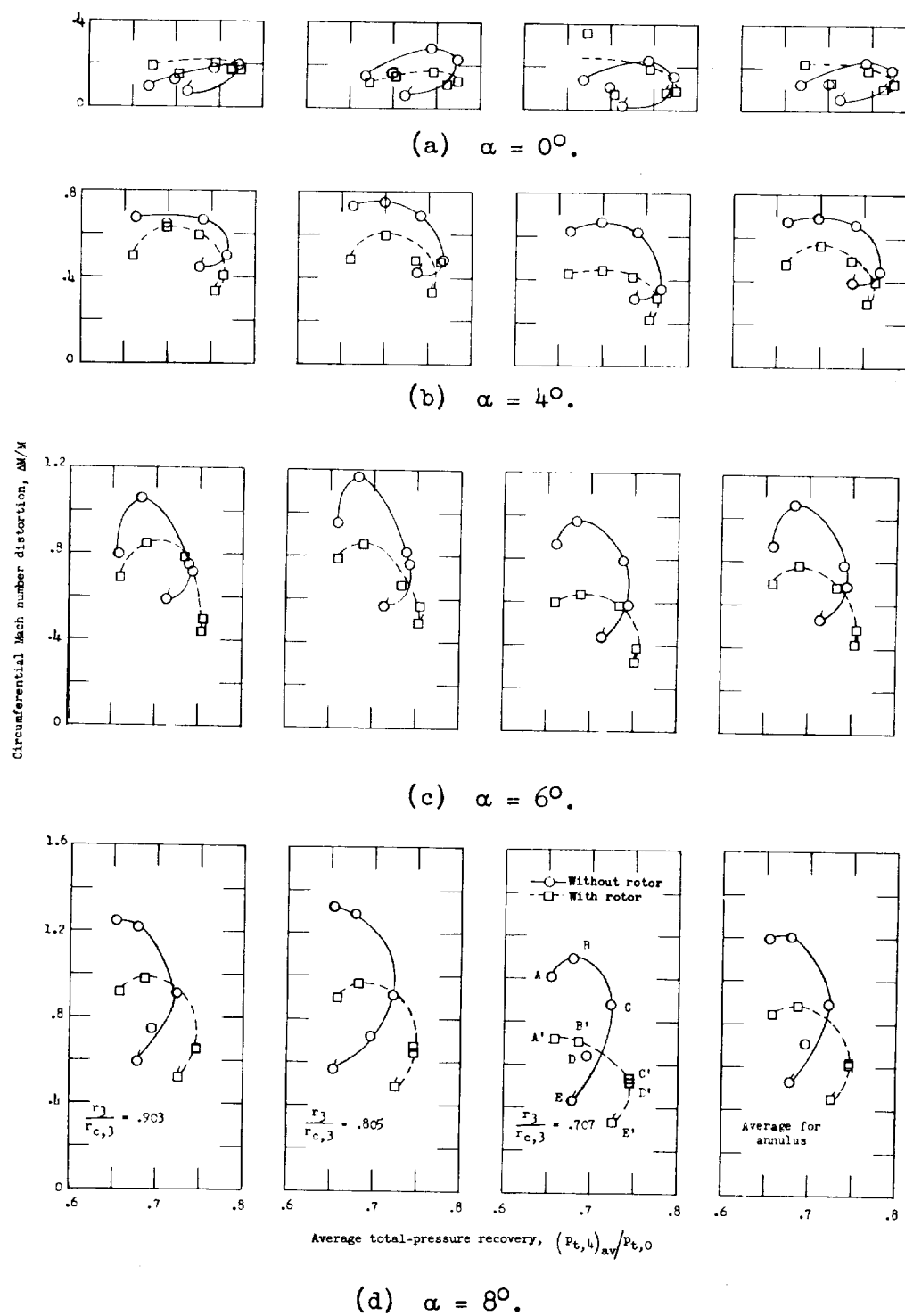
Figure 11.- Effect of freely rotating rotor on circumferential total-pressure distortion as a function of total-pressure recovery and angle of attack. Flagged symbols indicate buzz. Points A to E and A' to E' indicate back-pressure settings.
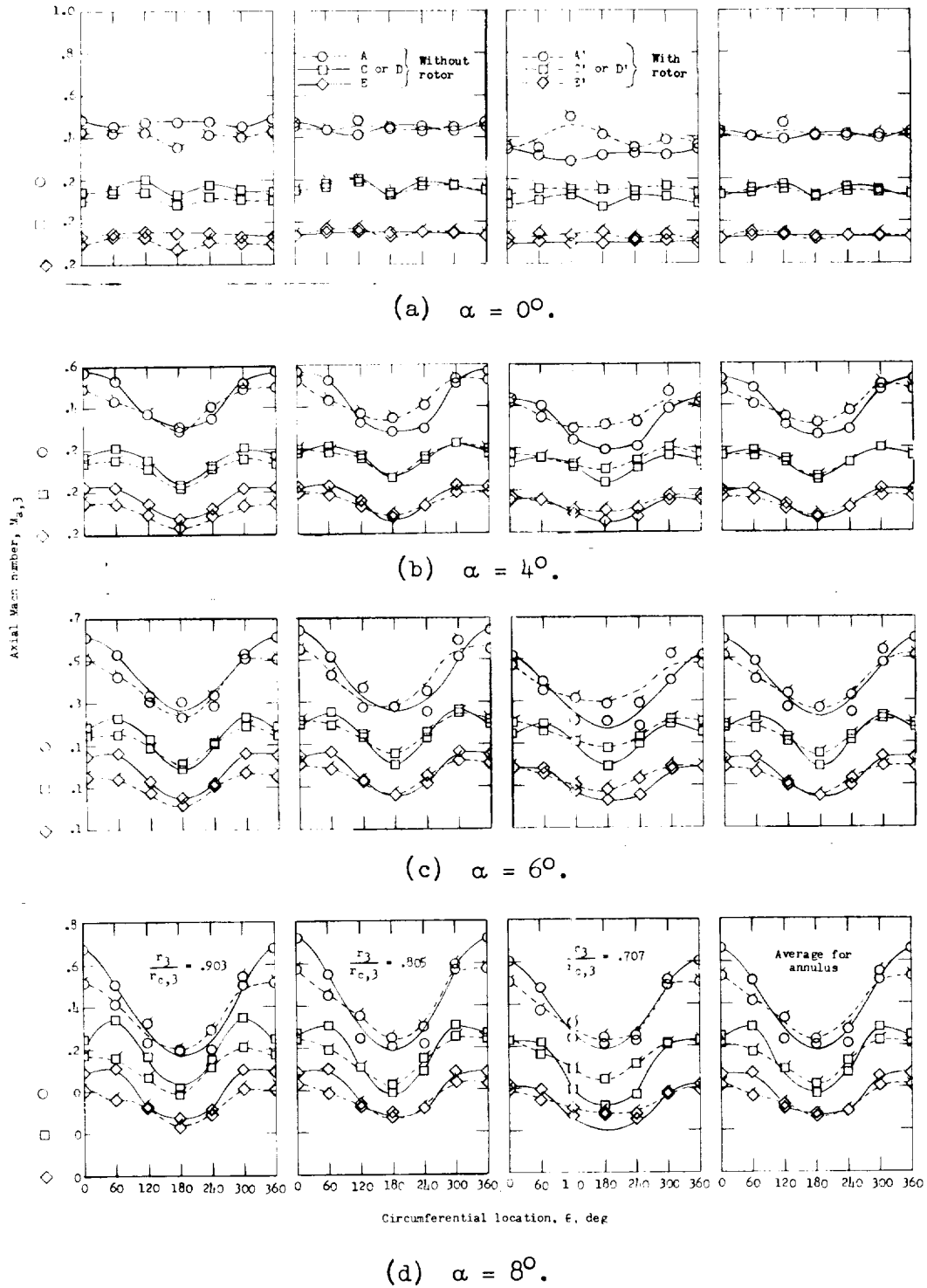
(a) $\alpha = 0°$.

(b) $\alpha = 4°$.

(c) $\alpha = 6°$.

(d) $\alpha = 8°$.
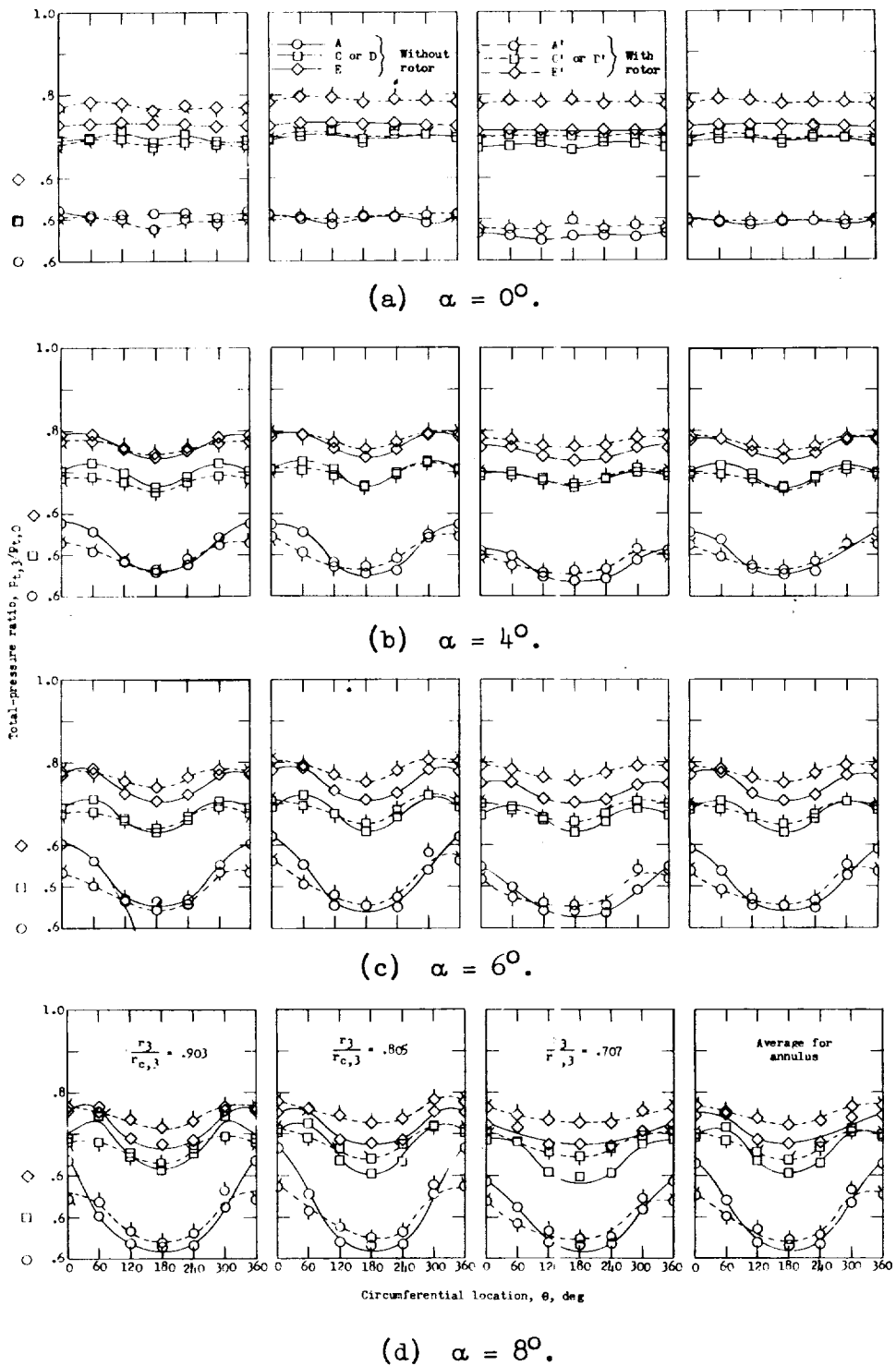
Figure 12.- Effect of freely rotating rotor on circumferential total-pressure ratio distributions as a function of angle of attack and back pressure.

Figure 13.- Average total-pressure recovery at station 3 with and without freely rotating rotor for all angles of attack and back pressures. Flagged symbols indicate buzz.

(a) $\dfrac{r_3}{r_{c,3}} = 0.903.$

(b) $\dfrac{r_3}{r_{c,3}} = 0.805.$

(c) $\dfrac{r_3}{r_{c,3}} = 0.707.$

(d) Average for annulus.

Figure 14.- Circumferential Mach number distortion with and without freely rotating rotor for all angles of attack and back pressure. Flagged symbols indicate buzz.

Figure 15.- Effect of freely rotating rotor on circumferential Mach number distortion as a function of total-pressure recovery and angle of attack. Flagged symbols indicate buzz. Points A to E and A' to E' indicate back-pressure settings.
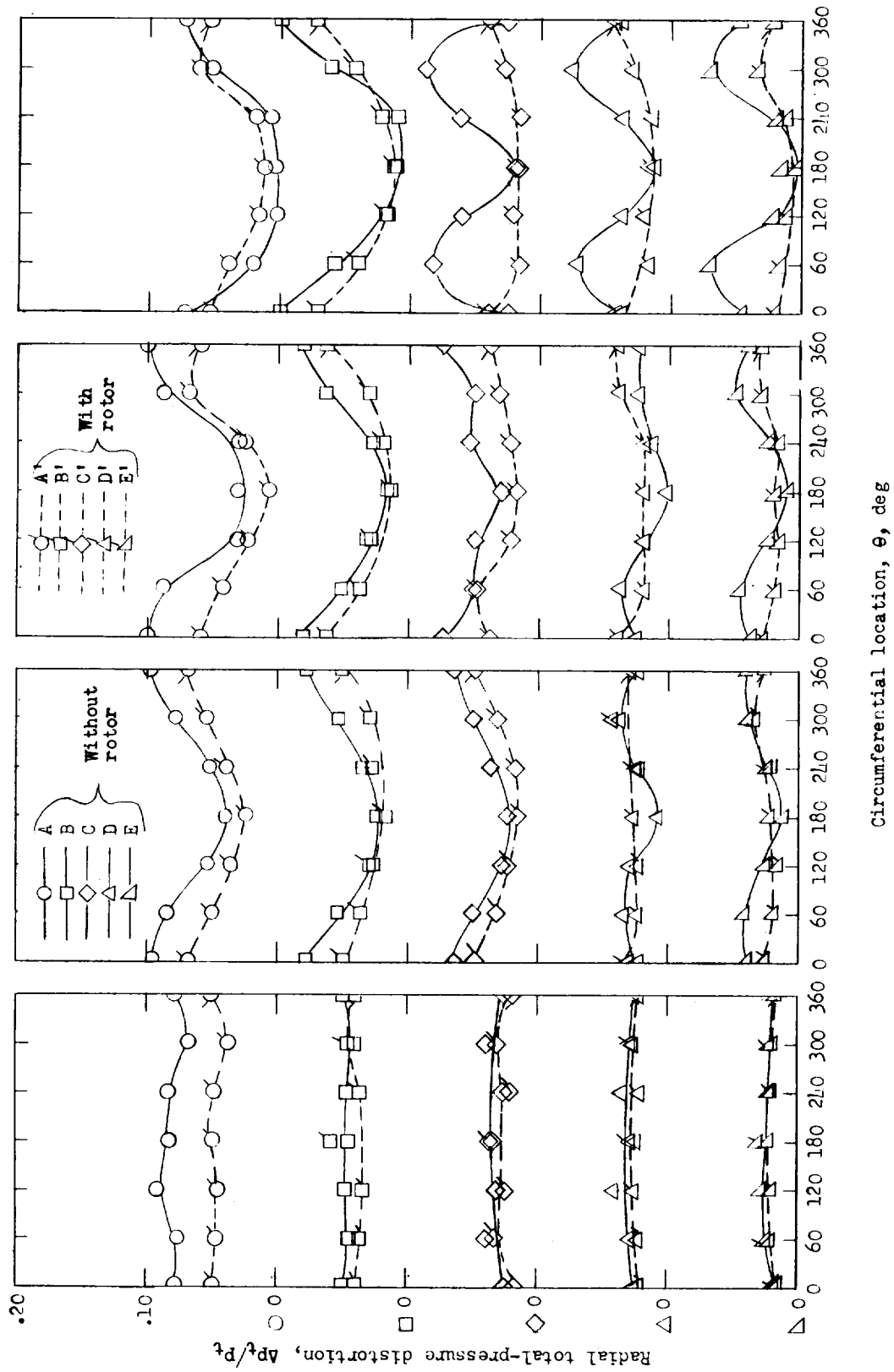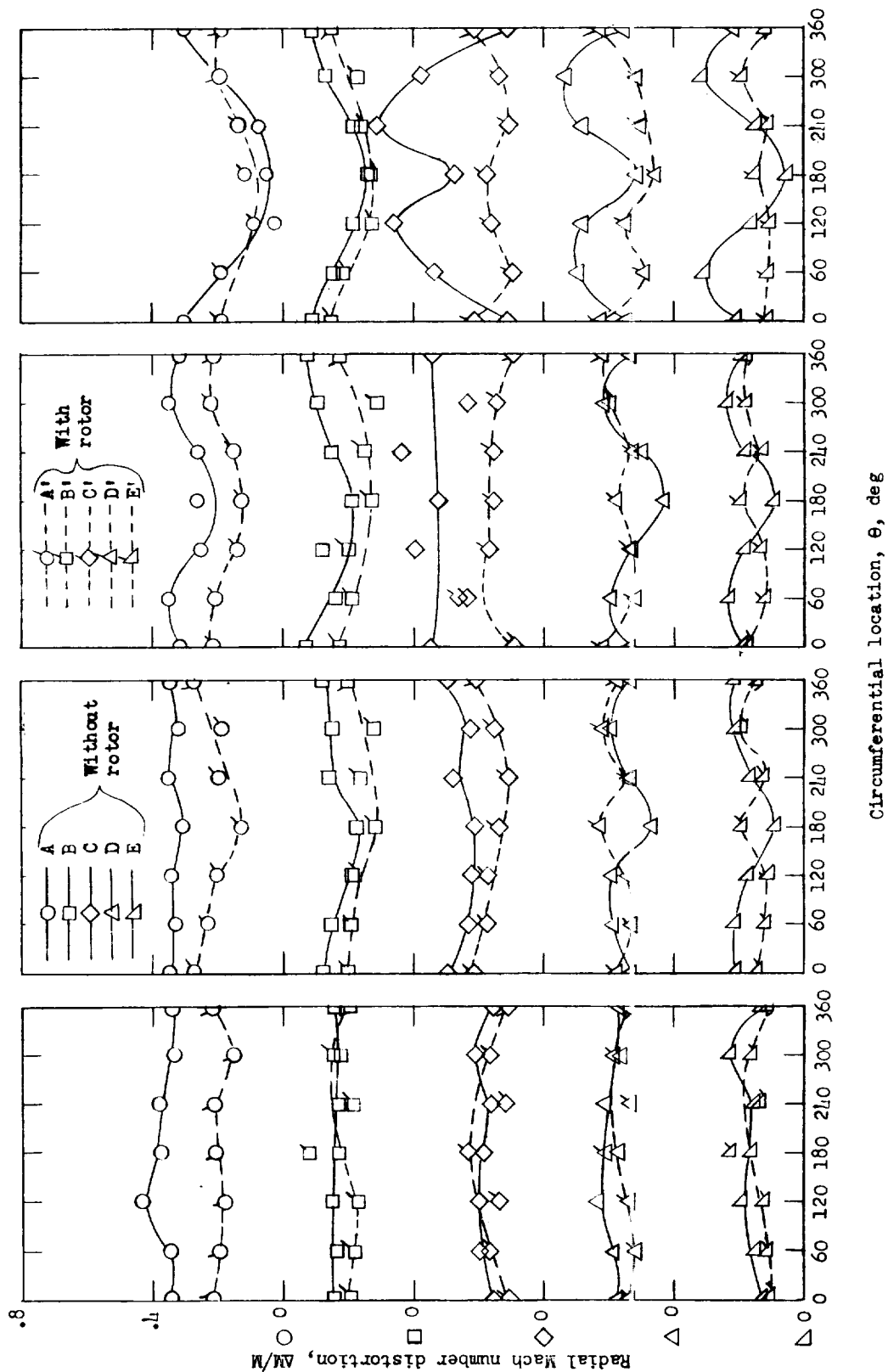
(a) α = 0°.

(b) α = 4°.

(c) α = 6°.

(d) α = 8°.

Figure 16.- Effect of freely rotating rotor on circumferential Mach number distributions as a function of angle of attack and back pressure.

Figure 17.- Effect of freely rotating rotor on radial total-pressure distortion as a function of angle of attack and back pressure.

(a) $\alpha = 0°$.   (b) $\alpha = 4°$.   (c) $\alpha = 6°$.   (d) $\alpha = 8°$.

Figure 18.- Effect of freely rotating rotor on radial Mach number dis-
tortion as a function of angle of attack and back pressure.

(a) α = 0°.   (b) α = 4°.   (c) α = 6°.   (d) α = 8°.

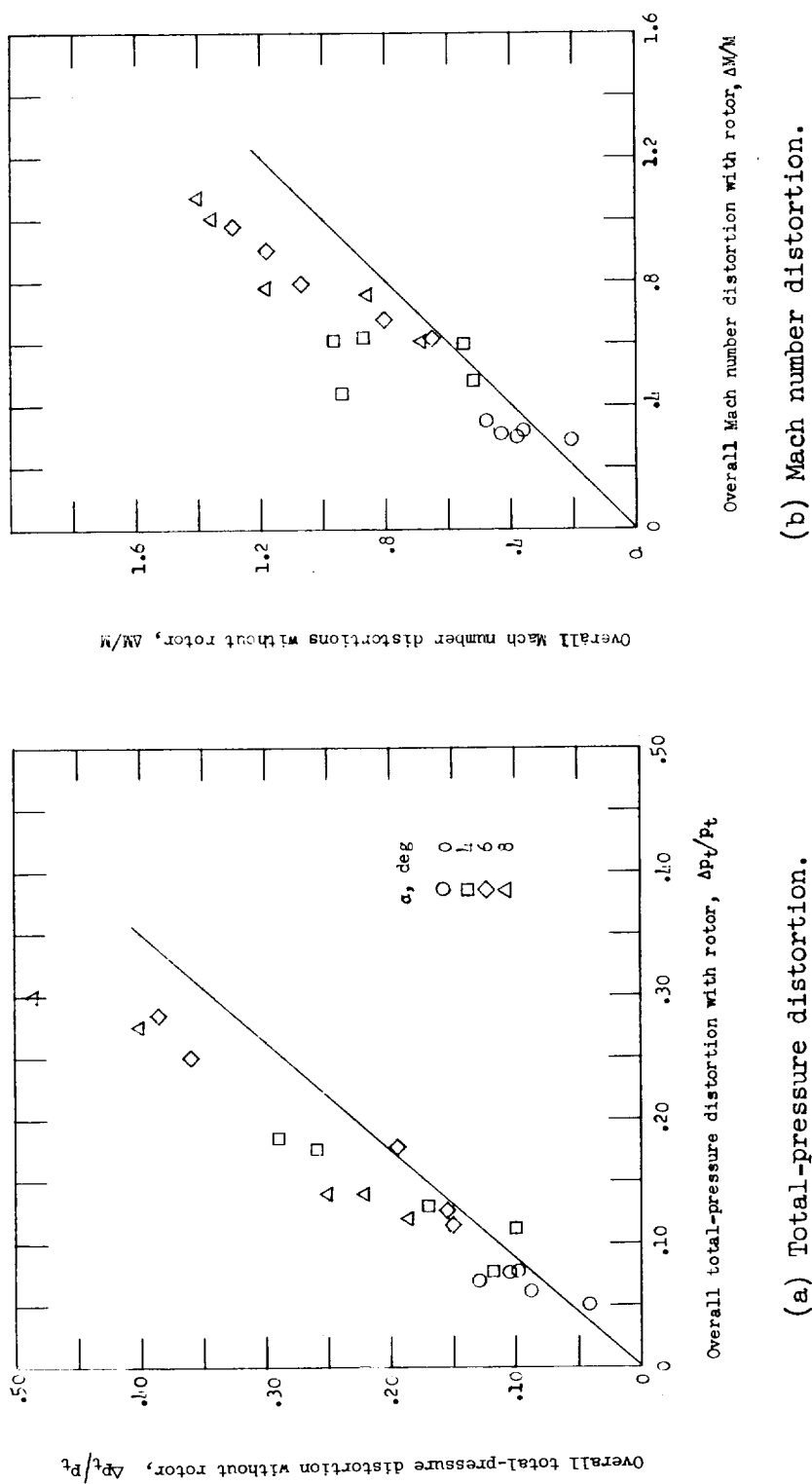(b) Mach number distortion.

(a) Total-pressure distortion.

Figure 19.- Effect of freely rotating rotor on overall distortions.